photonics

MDPI

Article

High-Capacity 16 × 10 Gbps Quad LP Modal MDM System Using an Integrated MMF-FSO Link Under Severe Climate Scenarios

Meet Kumari [1], Jyoteesh Malhotra [1] and Satyendra K. Mishra [2,*]

[1] Department of Electronics and Communication Engineering (ECE), National Institute of Technology Delhi, Delhi 110036, India; meetkumari@nitdelhi.ac.in (M.K.); jyoteesh@gmail.com (J.M.)
[2] SRCOM Division, Centre Technologic de Telecomunicacions de Catalunya, Castelldefels, 08860 Barcelona, Spain
* Correspondence: smishra@cttc.es

Abstract

Mode division multiplexing (MDM) is an emerging optical communication solution for high-capacity wired–wireless applications. Due to the presence of modal crosstalk and link impairments in MDM, this work aims to design a system that provides low complexity, an improved Shannon Capacity limit, and high spectral efficiency. In this work, a quad modal MDM system using an integrated parabolic index multimode fiber and free-space optics (PIMMF-FSO) link is presented. Four linearly polarized (LP) modes, LP_{01}, LP_{22}, LP_{03}, and LP_{13} based on a 16 × 10 Gbps MDM system offering different sixteen channels, are realized. Results show that the system can sustain a 7.5 dB insertion loss over 100 m FSO and a 100 m fiber range for different LP modes under the impact of clear air, moderate haze, heavy rain and wet snow climates with weak turbulence. A faithful fiber range of 3000 m can be obtained successfully in the proposed system with a −10 dB link loss, −7.62 dBm received power and 10 dB noise. Compared to existing designs, the proposed design offers optimum performance in terms of high channel capacity and a high traffic rate with low complexity and high spectral efficiency. Additionally, high received power, with acceptable noise, link loss, FSO misalignments and fiber nonlinearities, is successfully obtained.

Keywords: mode division multiplexing (MDM); free-space optics (FSO); multimode fiber (MMF); linearly polarized (LP)

1. Introduction

Recent developments in the expansion of internet subscribers have seen an exponential rise in terms of mobile users and a huge amount of information. Subsequently, the telecom sector supports approximately 21% of greenhouse gas (GHG) emissions, and its total power consumption is anticipated to reach higher levels by 2025. Hence, it is quite important to use a network that can connect a substantial number of different devices with the assurance of high-capacity and long-reach communication related to the latency, throughput, cardinality, and communication range between two end points [1].

Free-space optics (FSO) is a favorable wireless communication technology for an extensive range of wireless services and applications. FSO communication offers unlicensed data bandwidth higher than 100 Gbps. It also provides long-reach communication, inherent security and sustainability in electromagnetic interference [2]. However, atmospheric turbulence and link noise, along with signal intensity and phase variations in FSO links,

Check for updates

Received: 26 March 2026
Revised: 11 April 2026
Accepted: 16 April 2026
Published: 19 April 2026

Copyright: © 2026 by the authors. Licensee MDPI, Basel, Switzerland. This article is an open access article distributed under the terms and conditions of the Creative Commons Attribution (CC BY) license.

can cause huge power losses in propagating signals. Hence, it is highly important to use appropriate communication technology that can fulfil the needs of the dense deployment of the fifth generation (5G) and beyond in severe atmospheric conditions [1].

Further, the rapid growth of social networks, new data traffic, and rapid technology advancement requires extending the capacity of optical communication networks. However, the system capacity of conventional single mode fibers (SMFs) has reached the nonlinear Shannon capacity limit [3,4]. Currently, space division multiplexing scenarios in multimode fiber (MMF) have been presented to handle this capacity crunch. In the MMF-based systems, the presence of a mode division multiplexing (MDM) technique, which multiplexes the optical signals with distinct spatial modes, has been realized to considerably increase the channel capacity of optical fiber communication networks. However, the MDM systems suffer from both linear as well as nonlinear effects of MMF such as attenuation, modal dispersion, linear coupling and chromatic dispersion [5].

Furthermore, with the rise of increased throughput from emerging applications, fiber–FSO integration is expected to enable the achievement of different user-specified applications while increasing the physical layer capacity. In the last few years, an integrated fiber–FSO has become a significant communication technique for providing ultra-high and flexible speed when fiber is difficult or unavailable to deploy. It causes a last-mile bottleneck, as well as spectrum congestion issues [6]. It is also noteworthy that the widespread deployment of fibers cables in conventional optical networks may not be suitable for unconventional deployment scenarios like remote locations, difficult areas, rains, urban city centers, etc., where auxiliary fiber deployment may be restricted owing to restricted flexibility and high installation costs. Thus, integrated fiber–FSO is considered as one possible solution to mitigate the above issues [7].

1.1. Related Work

In previous work, a gigabit passive optical network (GPON) transmission using linearly polarized (LP) modes, LP_{01} and LP_{11}, over a 10 km few mode fiber (FMF), as well as SMF at 2.5 Gbps, has been demonstrated [8]. This system is cost effective and simple in design but also has a limited system capacity and data rate. In [9], an MDM with time division multiplexing passive optical network (TDM-PON) using reflective semiconductor optical amplifier (RSOA) was demonstrated. The results depict a 10 km FMF and 20 km SMF distance, at a 10/1 Gbps data rate. Nevertheless, it also adds to the system complexity and cost due to the use of an amplifier and orthogonal frequency division multiplexing (OFDM). In another work, a cascaded MDM-PON over 10–55 km over two few mode fibers (FMFs) and an MDM-based TDM-PON over 10 km FMF with 10 km SMF at 10 Gbps were successfully demonstrated [10]. However, to realize more modes, the mode multiplexer/demultiplexer (MUX/DEMUX) and FMF fabrication should be improved by using a multi-core technique in this system. A terahertz wireless scenario using four Laguerre–Gaussian (LG) modes, LG_2^0, LG_1^1, LG_0^3, LG_0^1, and LG_2^1, was demonstrated. It also carries a 2-Gbaud quadrature phase shift keying signal over a 40 cm FSO link at 8 Gbps [11]. The system performance can be enhanced by extending the FSO ranges by accommodating a higher transmission power, distinct diffraction patterns with high conversion efficiencies for all LG modes, and a larger receiver aperture to solve the issue of beam divergence. An OFDM-based wavelength division multiplexing (WDM) PON-FSO system over 20 km SMF fiber and 3000 m FSO link at 10 Gbps data rate was realized under moderate haze and heavy rain climate and weak to strong turbulence [1]. But this design will become complex and costly whenever the channel capacity is improved. In [12], an OFDM-MDM system using orbital angular momentum (OAM) modes was simulated at 120 Gbps, and the results depict that a faithful FSO range of 1.5 km under low dust

and 0.40 km under heavy dust can be obtained. Again, this system offers limited channel capacity under strong turbulence. In a 40/10 Gbps time and wavelength division multiplexing PON (TWDM-PON) using an OFDM scheme, over 25 km SMF is realized. This design incorporates limited link flexibility due to the use of a fixed fiber cable along with a complex OFDM receiver design [13]. In [14], a switching scheme based on an integrated FSO and radio frequency (RF) system with a selective decode-and-forward relay network was presented over a 3000 m range under clear air, haze and heavy rain scenarios. In [15], a ring topology-based WDM-PON at a 28 Gbps data rate was realized over a 25 km SMF and 2 m FSO range. However, the inclusion of optical couplers at the end units lead to critical power issues, which inhibit the system capacity. Moreover, a WDM-FSO system employing 940 m FSO and 51 km SMF range at 40 Gbps was realized [16]. Here, the FSO length can be extended by using an amplifier to compensate for the insertion losses.

1.2. Motivation and Contributions

In prior works, various high-speed and long-reach hybrid FSO–fiber link-based systems were realized by using complex multiplexing techniques such as OFDM, TDM, etc. The performance analysis of hybrid FSO–fiber systems is required to enhance high-capacity, cost-effective and less complex designs with more flexibility as well as reliability. From the perspective of 5G-based networks, the MDM technique is needed to address the imminent capacity crunch. It is also significant to investigate the impact of various climate conditions, turbulent effects, and FSO–fiber link impairments in a hybrid fiber–FSO system. In addition, the performance of the quad modal PIMMF-FSO system for sixteen different channels under severe climate conditions in terms of the link loss, noise, output noise, and received power has not been investigated yet. Further, the threshold insertion loss at bit error rate (BER) limit for FSO–fiber-integrated-based systems has not been investigated, and it is significant in order to obtain optical system performance along with other noise.

Thus, inspired by the MDM approach, which can be used in both fiber and FSO communication systems to improve the traffic rate, link capacity and to mitigate the effects of atmospheric scenarios, a quad LP modes-based MDM system is designed and investigated. With the exponential rise in data traffic, network service providers are experiencing numerous challenges, such as low latency, limited network capacity, high transmission rates, and higher deployment as well as maintenance costs. The fiber–FSO architecture is noted as a promising solution to minimize the above challenges [7]. The integration of parabolic index multimode fiber (PIMMF)-based backhaul and FSO-based fronthaul in an MDM system can exploit the benefit of both wireless and wired links to provide flexibility together with higher data rates. To date, MDM systems with multiple channels and multiple modes at high-speed over an integrated PIMMF-FSO link under the impact of diverse link impairments and atmospheric losses have not realized the enhancement of system capacity and flexibility.

In this paper, an MDM system employing an integrated PIMMF-FSO link under various climate conditions and losses is realized. In particular, (1) a switch selection technique is used for supporting long-reach transmissions with loss mode crosstalk and for high data security; (2) the system is validated by considering the impact of different climate and turbulence effects for different operating modes and wavelengths; (3) a high speed and high capacity transmission over an integrated fiber–FSO link is offered with a low cost and simple architecture design. The major contributions are as follows:

To design a four LP modal MDM system under PIMMF-FSO link impairments and turbulent conditions.

To evaluate the system performance for varied insertion losses and fiber ranges in terms of the BER, link loss, noise, and received power with the noise level in the system.

Compare the proposed system with existing ones based on the obtained results and different performance parameters.

The reminder of this work is organized as follows: the proposed design principle and simulation setup is described in Section 2. This section also depicts the generated modes and simulation specifications. Sections 3 and 4 analyze the obtained results and provide a detailed discussion, respectively. Section 5 summarizes the conclusions and key applications of the proposed architecture.

2. Proposed Design

The schematic of the MDM system using an integrated PIMMF-FSO link is depicted in Figure 1. Four different input wavelengths 1550–1552.4 nm with an 0.8 nm channel width are used. Here, each input wavelength is operated at four distinct LP modes, thus offering sixteen channels at an aggregate data rate of 160 Gbps (=10 Gbps bit rate × 4 modes × 4 wavelength channels). In this way, the MDM technique helps to increase the system capacity by using different operating modes at a single wavelength for numerous end users instead of using different wavelengths. At the transmitter (Tx) side, the signals from four sets of transmitters are multiplexed and selected at specific wavelengths using a select selection component. Then, the optical beam carrying several LP modes is launched into an integrated fiber–FSO link. After the link transmission, the signals are again selected at specific wavelength and then demultiplexed into individual mode signals. Neither the transmission link nor mode will generate larger crosstalk among different wavelengths and modes; so, the signal at each receiver can be separately detected without a coherent receiver. This architecture indicates the simplicity, as well as cost effectiveness, for multiple input signals.

The proposed architecture of 16 × 10 Gbps MDM system using an integrated PIMMF-FSO link incorporates four distinct LP modes. For transmission, four different wavelengths, 1550, 1550.8, 1551.6 and 1552.4 nm, are used at the transmitter, where each wavelength operates at four different LP modes. LP modes {LP_{01}, LP_{22}, LP_{03}, and LP_{13}} are generated using a continuous-wave (CW) laser source in conjunction with the multimode generator (MMG) component in the OptiSystem tool, which excites the supported spatial modes based on the specified PIMMF refractive index profile. LP modes are obtained by defining the refractive index profile of PIMMF, incorporating key parameters such as the core-cladding refractive index, core radius, numerical aperture (NA), and operating wavelength. The selected parameters for a standard PIMMF are given in Table 1. Additionally, the generated LP modes have been verified by analyzing their spatial intensity distributions with the standard theoretical LP mode profiles reported in the existing works [17–19].

At a specific wavelength, each transmitter incorporates a 10 Gbps non return to zero (NRZ) data format, which is modulated using the Mach–Zehnder modulator with an incoming signal from a spatial continuous wave laser. Spatial laser diodes allow the emergence of high powers (~100 mW) and the chance to be directly modulated at high frequencies (~25 GHz). The LiNbO3 Mach–Zehnder interferometers' modulator increases the bandwidth as well as the extinction ratio while reducing the insertion losses. In this system, NRZ encoding is utilized, as it offers a lower bandwidth requisite if compared to return to zero encoding [20]. For a single wavelength, a 4:1 MUX operating at 10 GHz bandwidth multiplexes all modulated signals. The insets show various LP modes generated at a specific spatial laser. Then, the signals selected by the select selection component are

passed through a PIMMF followed by an FSO link. The parabolic profile of PIMMF is described as follows [17–19]:

$$n^2(r) = \begin{cases} n_1^2\left[1 - 2\Delta\left(\frac{r}{a}\right)^2\right] & 0 \le r \le a \\ n_1^2[1 - 2\Delta], b \ge r > a \end{cases} \quad (1)$$

where the refractive index step (Δ) is equal to $\frac{n_1^2 - n_2^2}{2n_1^2}$, n_1 and n_2 define the refractive peak index parameter at the center and cladding of PIMMF, respectively, and a and $(b - a)$ are the core and clad radius, respectively. The effect of clear air, moderate haze, heavy rain, wet snow climate conditions and weak turbulence effects are considered on LP beams at an aggregate data rate of 160 Gbps.

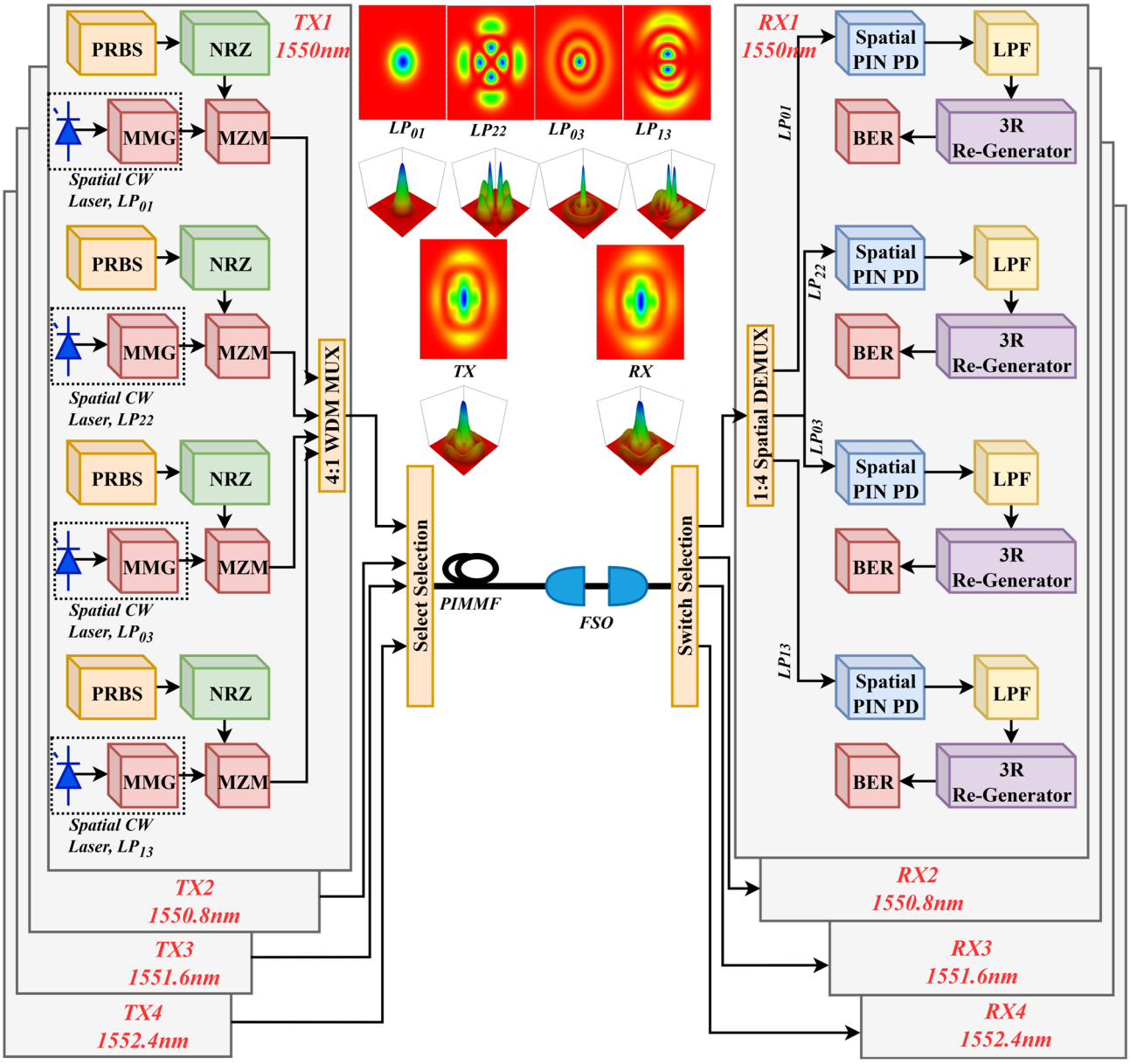


Figure 1. Proposed architecture of quad MDM modal-integrated 16 × 10 Gbps PIMMF-FSO system under diverse climate scenarios; insets: transmitted and received LP modes.

At receiver (Rx), the received signals are firstly selected by switch selection followed by four 1:4 spatial DEMUX for different operating modes at a specific wavelength. Each

spatial optical receiver incorporates a spatial PIN photodiode (PD) for direct detection, whereas a low pass filter (LPF) is followed for reducing the signal noise. A 3R regenerator is utilized to improve the signal quality. The BER performances are evaluated via a BER analyzer. The insets show the obtained optical spectrum at the Tx and Rx side for a 1550 nm operating wavelength. Various phase profiles of the generated LP modes at the Rx side are also shown in Figure 2.

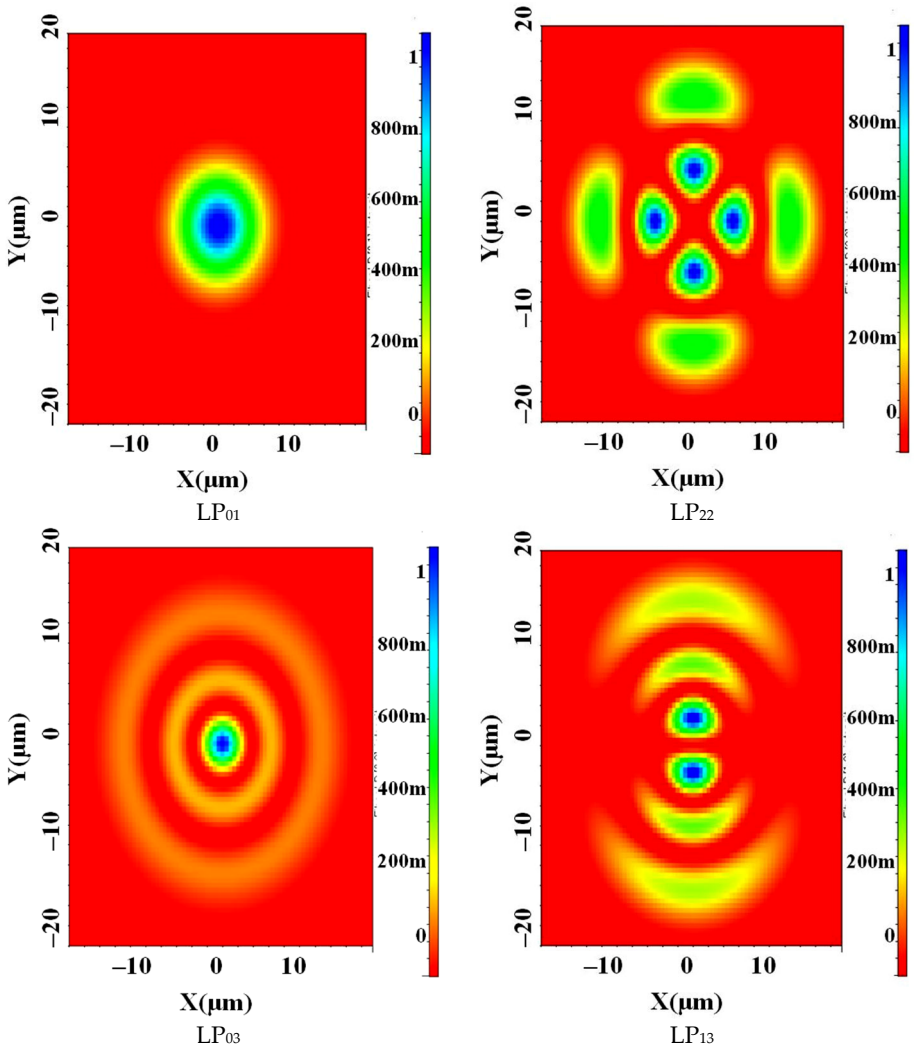


Figure 2. Intensity profile of generated modes in the proposed system.

The generated LP modes' intensity profiles are depicted in Figures 2 and 3. Spatial visualizer is used to present both the intensity and phase profiles of LP_{01}, LP_{22}, LP_{03}, and LP_{13} in 2D and 3D-view. It also calculates and lists the label, power, and wavelength for each LP mode profile. These profiles help to determine the various properties of each LP mode at a specific wavelength. Figure 2 depicts the intensity profiles of the LP_{01}, LP_{22}, LP_{03}, and LP_{13} modes having (l = 0, m = 1), (l = 2, m = 2), (l = 0, m = 3) and (l = 1, m = 3) mode indices in X or Y polarizations. For fundamental mode LP_{01}, the highest power is observed at the center, which indicates maximum transmission capacity over a long reach. The lowest order mode (LP_{01}) has an intensity profile similar to a Gaussian beam. The different color indicates the distinct signs of an electric field in a LP mode. The LP_{01} mode covers a large portion of the core area with a single ring, the LP_{03} mode is more focused in three rings, while both the LP_{22}, and LP_{13} modes have an azimuthal variation in intensity.

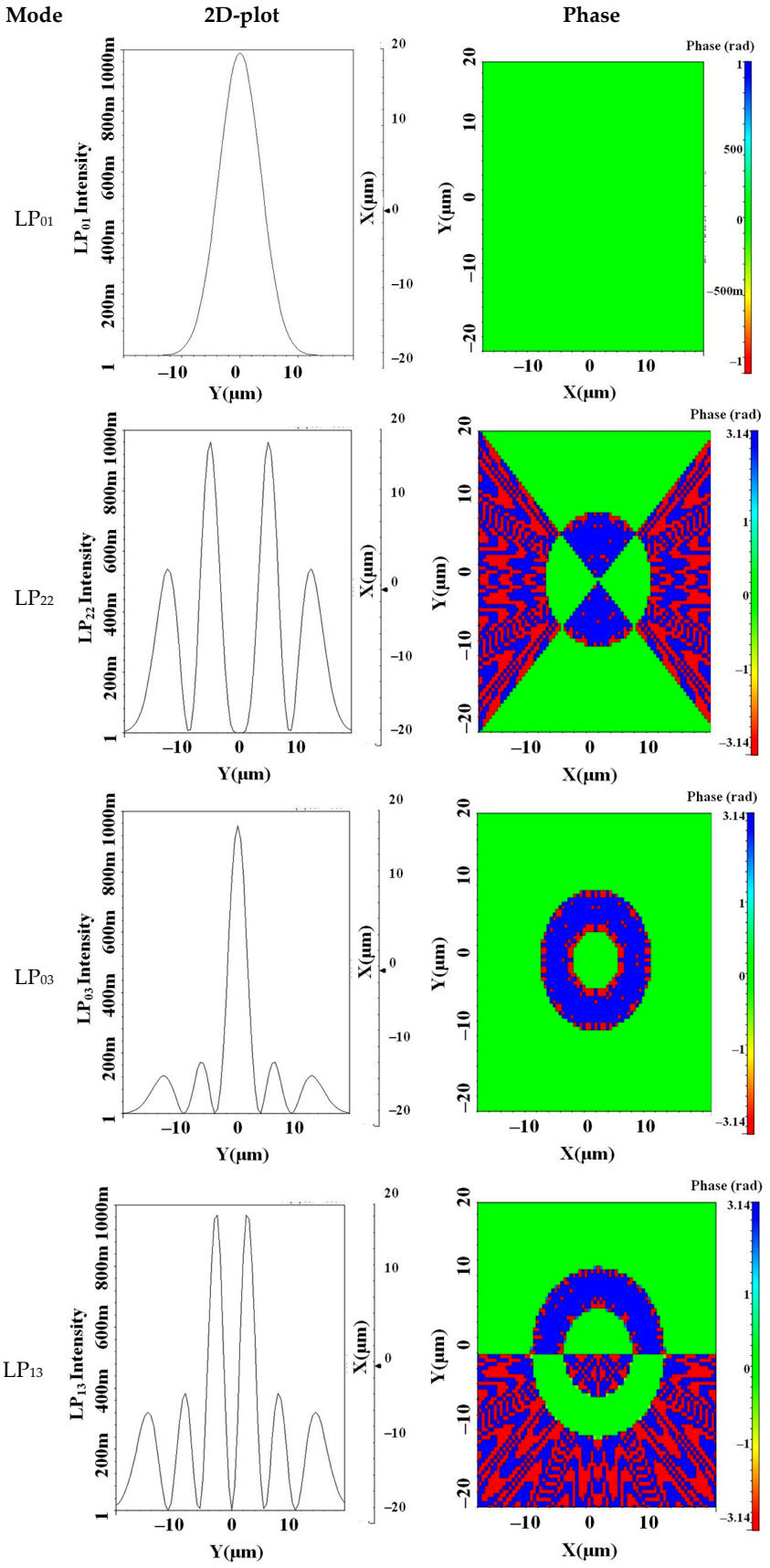


Figure 3. 2D-plot intensity and phase profile of generated modes in the proposed system.

Figure 3 depicts the 2D plot of various LP modes in terms of the amplitude of intensity profile. Here, a single central high-intensity lobe in LP_{01}, two high-intensity lobes

accompanied by two lower-intensity lobes in LP_{22}, one dominant lobe with four weaker surrounding lobes in LP_{03}, and two high-intensity lobes along with two lower-intensity lobes in LP_{13} are generated. For a higher 'm' value, the subsequent radial functions can oscillate in the core area of the fiber, while it diminishes in the cladding. In addition, the phase profiles present the variation in phase (rad) of different LP modes while propagating through PIMMF. It also indicates that the LP_{01} mode > 90% of power propagates within the core, but other higher order modes offer <50–90% power in the core.

The system is proposed and investigated in OptiSystem V.22, and its parameter specifications are depicted in Table 1.

Table 1. Simulation specifications [14,21].

Component	Parameters	Value	Unit
CW Laser	Wavelengths	1550, 1550.8, 1551.6, 1552.4	nm
	Linewidth	10	MHz
	Launch power	10	dBm
PRBS Generator	Bit rate	10	Gbps
MMG	Modes	LP_{01}, LP_{22}, LP_{03}, LP_{13}	
MZM Modulator	Extinction ratio	30	dB
PIMMF	Range	100–3000	m
	PIMMF attenuation	2.61	dB/km
	Core radius	25	μm
	Cladding radius	35	
	Refractive index peak	1.4142	
	Refractive index step	1%	
	Sellmeier approximations	Yes	
	Zero dispersion slope	0.97	ps/(nm^2.km)
FSO	Range	100	m
	Additional losses	0.01	dB
	Geometrical loss	Yes	
	Transmitter/Receiver aperture diameter	20	cm
	Beam divergence	2	mrad
	Transmitter/Receiver loss	0.1	dB
	Index refraction structure	10^{-17}	$m^{-2/3}$
	Scintillation model	Gamma–Gamma	
Spatial PIN PD	Shot noise	Yes	
	Responsivity	0.9	A/W
	Thermal noise	10^{-24}	W/Hz
	Dark current	10	nA
	Insertion loss	1–8	dB
LPF	Cutoff frequency	7.5×10^9	Hz
	Depth	100	dB

3. Results and Analysis

The proposed architecture is investigated in the widely accepted OptiSystem simulation software. The system performance is analyzed for four wavelength channels at different modes. Each wavelength operates at four LP modes to transmit the information over a fixed FSO range of 100 m and a variable PIMMF range of 100–3000 m at a 160 Gbps data rate.

Figure 4a–d shows the BER performance of the 1550 nm wavelength channel at LP_{01}, LP_{22}, LP_{03}, and LP_{13} modes for varied insertion in an integrated fiber–FSO link under diverse climate conditions at a 1550 nm wavelength channel. The system performance is calculated under diverse climate conditions and weak atmospheric turbulence using the Gamma–Gamma (GG) model. This model provides versatile access that can be realized

across an extended turbulence spectrum, from weak to strong turbulence regimes, and it is given as follows [1]:

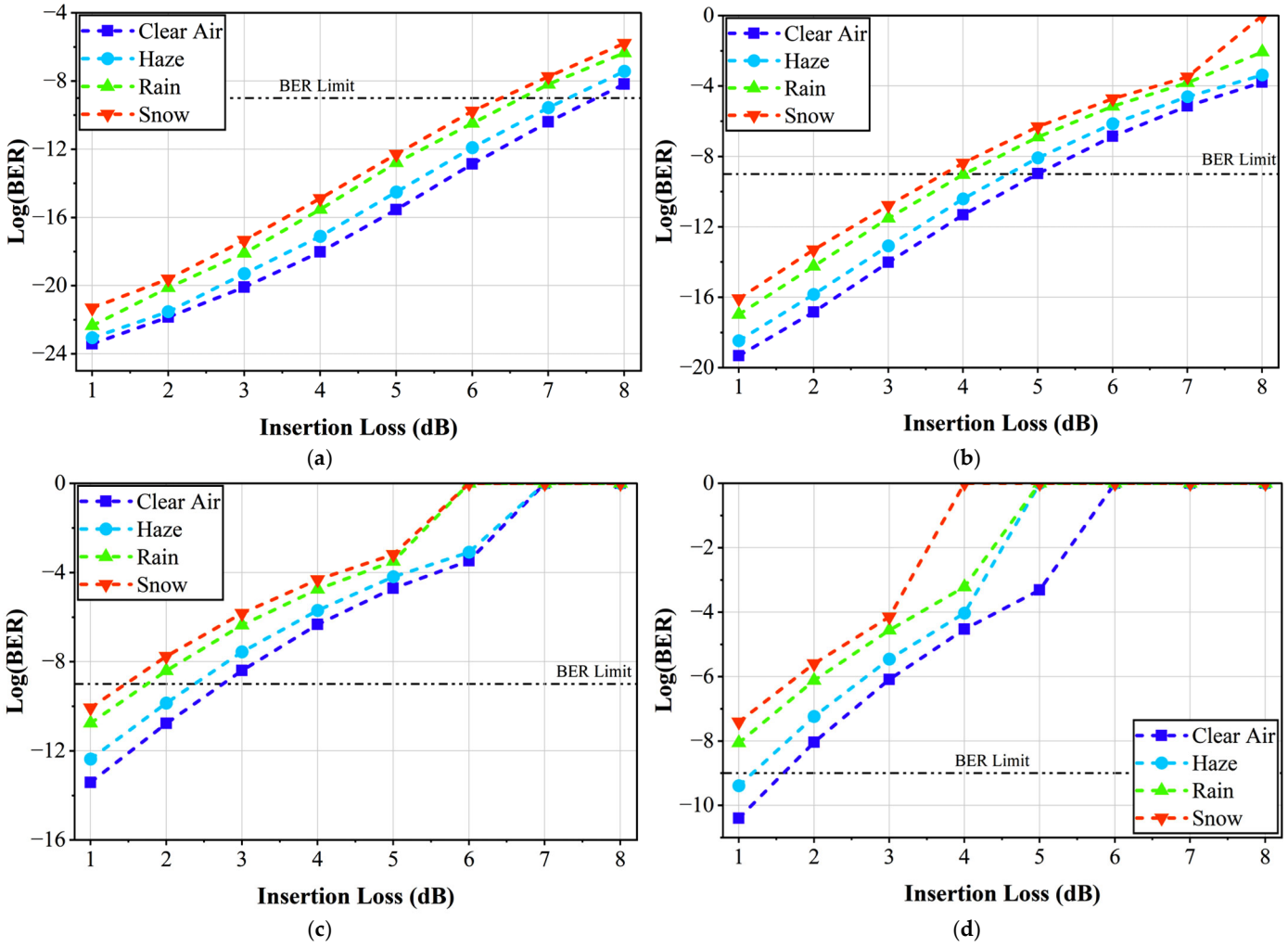


Figure 4. Insertion loss vs. BER for (**a**) LP_{01}, (**b**) LP_{22}, (**c**) LP_{03}, and (**d**) LP_{13} modes under diverse climate scenarios in the proposed system.

$$f_g(g) = \frac{2(lv)^{\left(\frac{l+v}{2}\right)}}{\Gamma(l)\Gamma(v)} \cdot g^{\left(\frac{l+v}{2}\right)-1} K_{l-v}\left[2(lvg)^{\frac{1}{2}}\right] \tag{2}$$

where $\Gamma(.)$ indicates the Gamma function, and K_{l-v} is the modified Bessel function of order $(l-v)$. l and v signify large and small scale effective eddies considerably, given as [1]

$$l = \frac{1}{\left[exp\left\{\frac{0.49k_0^2}{\left(1+0.18d^2+0.56k_0^{\frac{12}{5}}\right)^{\frac{7}{6}}}\right\} - 1\right]} \tag{3}$$

and

$$v = \frac{1}{\left[exp\left\{\frac{0.51k_0^2\left(1+0.18d^2+0.56k_0^{\frac{12}{5}}\right)^{\frac{-5}{6}}}{\left(1+0.90d^2+0.62d^2k_0^{\frac{12}{5}}\right)^{\frac{5}{6}}}\right\} - 1\right]} \tag{4}$$

Moreover, the FSO link under distinct climate conditions can be given as

$$P_{rx} = P_{tx} \cdot \left(\frac{A_r}{(\theta L)^2} \right) \cdot exp(-\alpha L) \tag{5}$$

where P_{rx} and P_{tx} indicate the respective power as transmitted and received, A_r is the effective aperture area at the receiver, L is the FSO range, θ is the beam divergence. and α depends on the weather conditions [22,23]. The FSO transmission is mostly unaffected by wet snow and heavy rain, as particle size is larger than the wavelength. However, wet snow is more destructive than heavy rain due to the big droplet size [24]. The heavy rain attenuation coefficient α_{rain} is given as [25]

$$\alpha_{rain} = \beta R^s \tag{6}$$

where R is the heavy rain rate, and β and s are coefficients depending on the operating wavelength as well as the temperature. Sources like smoke, dust and other particles, which are distributed in the surroundings, generate particulate matter called haze. The emergence of this matter to gaseous pollutants results in specific chemical reactions. As the size of the haze particles is comparable to the size of the transmitted signal wavelength, the effect is consequently classified as Mie Scattering [26]. The Beer–Lambert Law is widely utilized to calculate haze attenuation as [25]

$$\alpha_{haze} = e^{-\sigma L} \tag{7}$$

where σ means the haze attenuation coefficient.

Further, snow is categorized as wet and dry wet snow on the basis of the liquid equivalence ratio. The level of wet snow attenuation is identified by its visibility and particle sizes. The wet snow attenuation in terms of the wet snow rate, T (mm/hr), is defined as [27]

$$\alpha_{snow} = j \cdot T^k \tag{8}$$

where j and k present the wet snow coefficients based on dry and wet snow. For dry snow, $j = 5.42 \times 10 - 5 \times \lambda + 5.4958776$, and $k = 1.38$. While for wet snow, $j = 1.023 \times 10 - 4 \times \lambda + 3.7855466$, and $k = 0.72$ [27]. Again, the wet snow attenuation coefficient in terms of visibility range, V is given as [28]

$$\alpha_{snow} = 58/V \tag{9}$$

The BER performance of the system with respect to the signal-to-noise ratio, SNR, is given as [25]

$$BER = \frac{1}{2} erfc \sqrt{\frac{SNR}{8}} \tag{10}$$

Table 2 depicts the various climate conditions considered in the proposed system.

Table 2. Atmospheric conditions [29].

Atmospheric Condition	Value (dB/km)	Precipitation (mm/hr)
Clear air	0.2	
Moderate haze	4	
Heavy rain	10	25
Wet snow	13.73	

In Figure 4a–d, the 100 m fiber and 100 m FSO length is considered under the impact of weak turbulence. For a threshold BER of 10^{-9}, the system can sustain maximum 7.5, 7.2, 6.6, and 6.4 dB insertion loss under clear air, moderate haze, heavy rain, and wet snow

climates for LP_{01} mode, as depicted in Figure 4a. The acceptable insertion loss of LP_{22} mode under air, moderate haze, heavy rain and wet snow climates is 5, 4.6, 4 and 3.8 dB, respectively, as depicted in Figure 4b. Whereas for the LP_{03} mode, the BER limit can be obtained at 2.7, 2.3, 1.8 and 1.5 dB under air, moderate haze, heavy rain and wet snow conditions, respectively, as explored in Figure 4c. Moreover, Figure 4d depicts that the LP_{13} mode undergoes the least insertion loss tolerance as 1.5, 1.2 and <1 dB under air, moderate haze, heavy rain and wet snow climates, respectively. The observed transmission performance difference between the LP_{01}, LP_{22}, LP_{03}, and LP_{13} modes shows that the impairment for the mode LP_{13} is exceeding that for LP_{03}, followed by LP_{22} and LP_{01}. The severe climate conditions such as heavy rain and wet snow are not optimum for higher order modes. Moreover, the results indicate that link impairment due to modal crosstalk through integrated MMF-FSO transmission considering high insertion loss is notably high. Higher-order modes incorporate wider multi-lobed spatial distributions as well as weaker confinement, making them more sensitive to beam scattering, beam divergence, and turbulence-induced coupling in free space. This gives rise to increased modal crosstalk, high link attenuation, and accordingly degraded BER performance as compared to lower-order modes.

Further, mode coupling occurs due to the mismatch between the input field and a single mode, causing the power to distribute among multiple modes by the overlap integral. The coupling coefficient c_i is calculated as [30,31]

$$c_i = \int_0^{2\pi} \int_0^{\infty} E_{in}(r, \varnothing) E_i(r, \varnothing) r dr d\varnothing \tag{11}$$

where $E_i(r, \varnothing)$ indicates the mode's spatial profile, and $E_{in}(r, \varnothing)$ indicates the spatial input field. The coupling coefficient presents the overlap between the input field and modal field. The free-space disturbances alter the input field, leading to a change in overlap and causing power distribution, which is more pronounced for higher-order modes owing to their complex spatial profiles.

The eye patterns for the 1550 nm wavelength channel using LP_{01} mode at 1 and 8 dB insertion loss under diverse climate conditions are depicted in Figure 5. After the transmission at 8 dB insertion loss, the signals become worse than the signal at the 1 dB insertion loss. This can be attributed to the high power coupling at the LP_{01} mode than higher order modes and low modal crosstalk between all modes during transmissions as well as mode multiplexing/demultiplexing under different climates. In addition, clear and open eye patterns are seen under clear air followed by moderate haze, heavy rain and wet snow. The summarized results are depicted in Table 3.

Figure 6a–d shows the BER characteristic with respect to the MMF distance for different wavelength channels at the LP_{01}, LP_{22}, LP_{03}, and LP_{13} modes over 100 m FSO range under clear air. The BER performance is calculated firstly at the LP_{01} mode, where the faithful distance of 3000 m is obtained for the 1550, 1550.8, 1551.6 and 1552.4 nm wavelengths, as depicted in Figure 6a–d. The maximum fiber distance at a BER of 10^{-9} of 2100 m is obtained for the LP_{22} mode at the 1550, 1550.8 and 1551.6 nm wavelengths, as depicted in Figure 6a–c, while at 1552.4 nm, the faithful fiber range is <2100 m, as shown in Figure 6d. The higher order mode LP_{03} undergoes limited fiber range (even less than at LP_{22} mode), which is followed by the LP_{13} mode. Higher modes experience more power loss such as LP_{22} and LP_{03}, and LP_{13} has a low BER performance compared to LP_{01}. This is owing to the larger beam divergence and larger beam size, as well as the lower conversion efficiency for the LP beam generation.

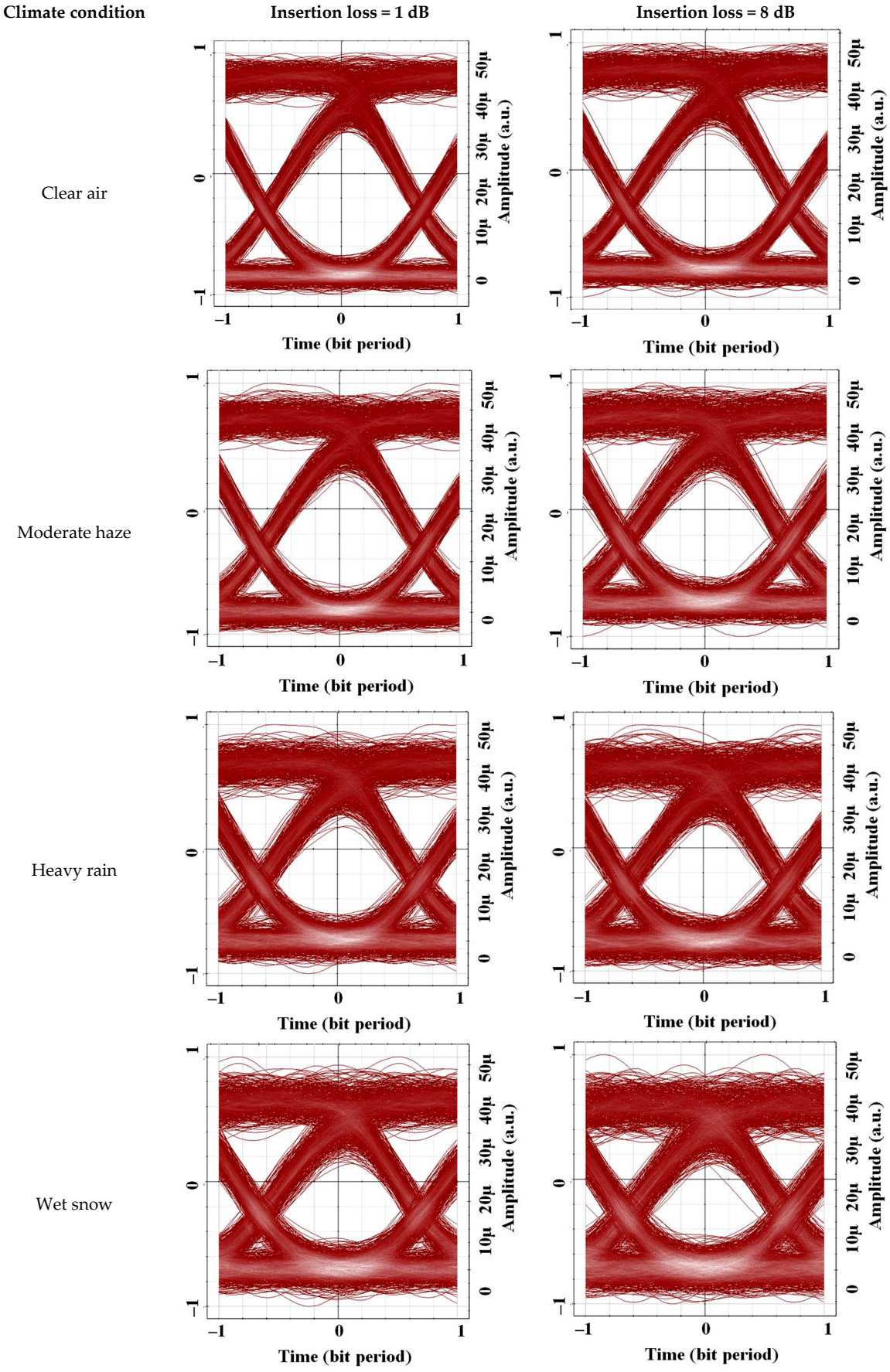


Figure 5. Eye patterns for LP_{01} mode at 1 and 8 dB insertion loss under diverse climate conditions.

Table 3. Summarized results for varied insertion loss under diverse climates for various LP modes.

Climate	LP_{01}	LP_{22}	LP_{03}	LP_{13}
	Insertion Loss (dB)			
Clear air	7.5	5	2.7	1.5
Moderate haze	7.2	4.6	2.3	1.2
Heavy rain	6.6	4	1.8	<1
Wet snow	6.4	3.8	1.5	<1

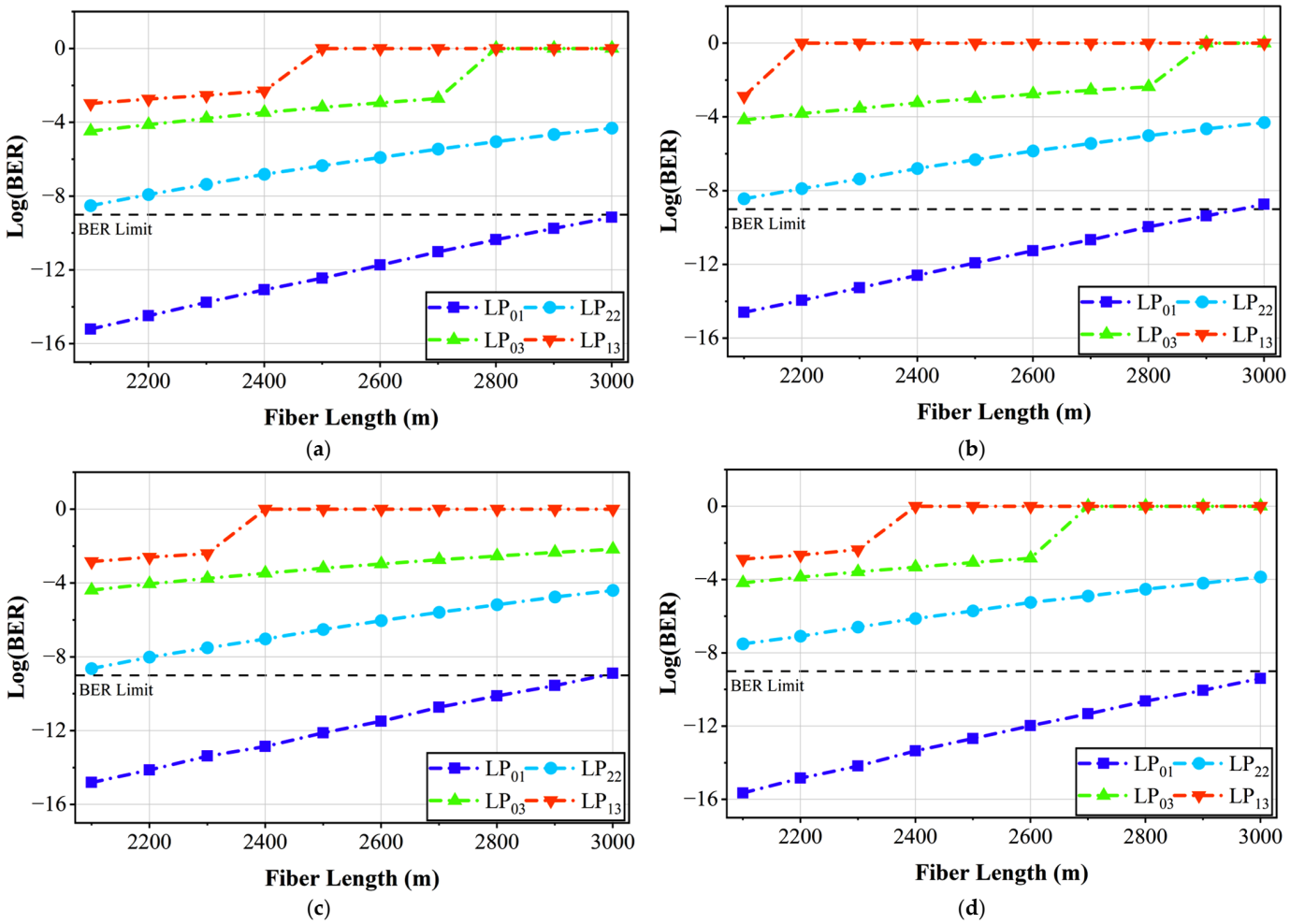


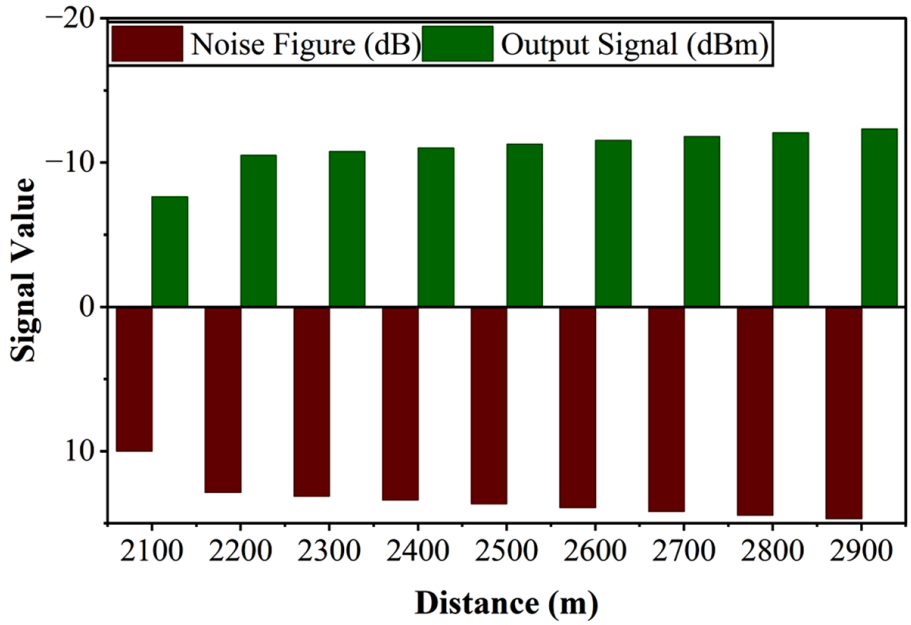
Figure 6. MMF length vs. BER at (**a**) 1550 nm, (**b**) 1550.8 nm, (**c**) 1551.6 nm and (**d**) 1552.4 nm for different LP modes under clear air climate.

Figure 7a,b depict the comparisons between the obtained noise, output signal, link loss and output noise over the 2100–3000 m fiber and 100 m FSO range at 1550 nm at LP_{01} under a clear air climate. For a varying fiber range, the noise increases from 10 to 14.7 dB, and the output signal decreases from −7.62 to −12.32 dBm, as depicted in Figure 7a. For the same fiber length, the signal experiences larger attenuation, resulting in an increased link loss from −10 to −14.70 dB, while the corresponding noise at the receiver also increases from −56.38 to −62.66 dBm, as depicted in Figure 7b. This implies that the link loss indicates the received signal strength, while the noise, as well as the output noise, quantify the signal quality degradation, collectively showing the overall system performance.

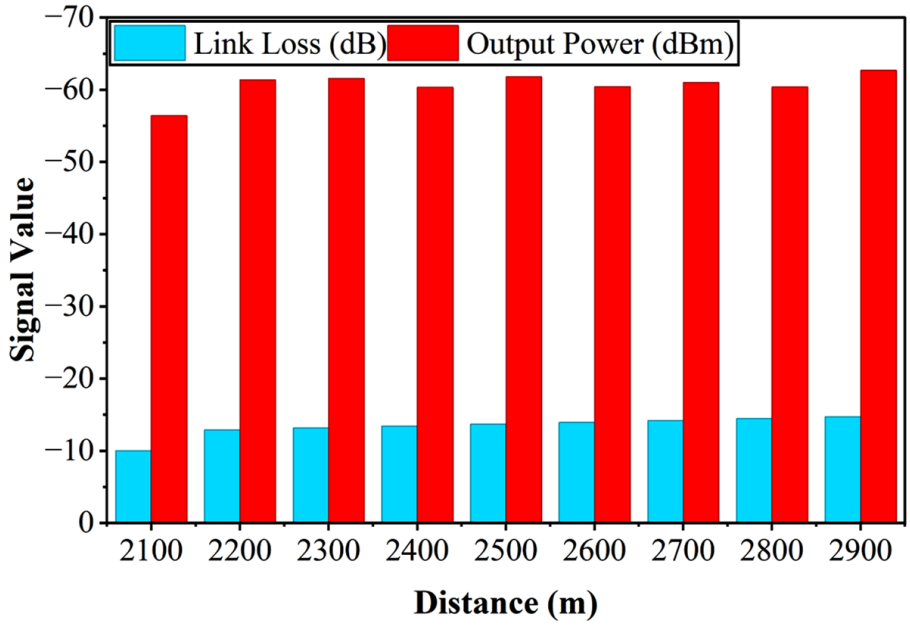
$$Link\ Loss = 10log_{10}\left(\frac{Input\ Power}{Output\ Power}\right)\ \text{dB} \quad (12)$$

and

$$Noise\ Figure = 10log_{10}\left(\frac{Input\ SNR}{Output\ SNR}\right)\ \text{dB} \tag{13}$$



(**a**)



(**b**)

Figure 7. System performance for varied fiber length with respect to (**a**) noise and output signal and (**b**) link loss and output noise at 1550 nm at LP_{01} under clear air climate.

Figure 8a–d depicts the 3D BER patterns of the LP_{01}, LP_{22}, LP_{03}, and LP_{13} modes at 1550 nm over 100 m MMF and a 100 m FSO range under clear air scenario.

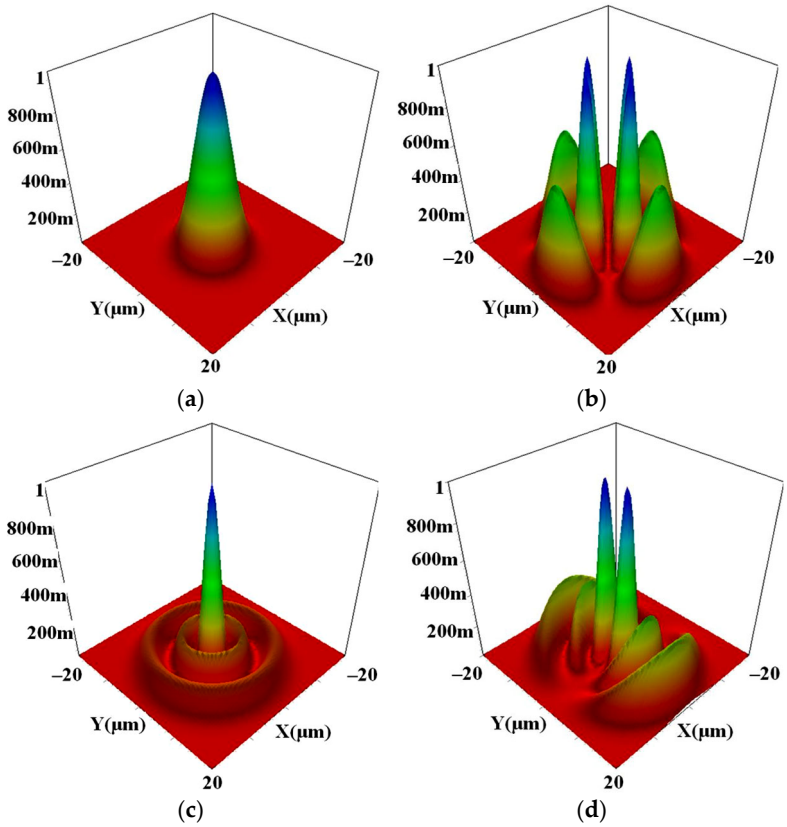


Figure 8. 3D profiles of (**a**) LP_{01}, (**b**) LP_{22}, (**c**) LP_{03}, and (**d**) LP_{13} modes at 1550 nm under clear air scenario in the proposed system.

Table 4 depicts the comparative analysis of the proposed design with respect to the existing works in terms of the fiber distance, wireless range, data rate and MDM modes under the impact of different climate conditions along with the major limitations. The proposed system is compared for both the simulation- and experimental-based systems. It is clear that the proposed system offers the highest system capacity of sixteen channels resulting in an aggregate data rate of 160 Gbps (=16 × 10 Gbps), as compared to the previous works, except Ref. [32], which realized just a 30 m range. A longer wireless range of 100 m is obtained than in Refs. [11,15]. Refs. [1,14,16,33] offer a better wireless range but with a more limited channel capacity than the proposed system. Refs. [1,8,9,13,15,16,33] offer a longer fiber range using SMF than the proposed work (PIMMF range=3000 m), but climate conditions are not considered in the former.

However, the proposed MDM system using an integrated fiber–FSO system offers a higher channel capacity, high data rate, simple design and cost-effectiveness, as compared to the other existing systems. By considering the tradeoff between the distance and transmission rate, the fiber range can be extended by using an optical amplifier. In the proposed system, erbium-doped fiber amplifiers (EDFAs), semiconductor optical amplifiers (SOAs), RSOAs and Raman amplifier (RAs) can be used. EDFAs operate near 1550 nm, but their cost is nonetheless a strong limitation. SOAs offer high flexibility and a large gain in bandwidth; however, their technology has not still reached maturity. RAs seem to present a better solution due to the high flexibility in selecting an amplification wavelength range, even though a large pump power is requisite to attain the large gain. RSOA offers a high gain and an enhanced power budget [20].

Table 4. Comparison analysis with respect to the existing works.

Design	Realization	Fiber Distance	Wireless Range	Data Rate	MDM	Climate	Limitation(s)
GPON-MDM [8]	Experimental	10 km (FMF) + 10 km (SMF)	-	2 × 2.5 Gbps	LP_{01}, LP_{11}	-	Limited flexibility, low data rate
MDM-TDM PON [9]	Experimental	10 km (FMF) + 20 km (SMF)	-	10/1 Gbps	LP_{01}, LP_{11}	-	Limited flexibility, low data rate, low capacity
FSO [11]	Experimental	Not used	40 cm	8 Gbps	LG_2^0, LG_1^1, LG_0^3, LG_0^1, LG_2^1	-	Limited distance, low data rate
PON [13]	Experimental	25 km (SMF)	-	40/10 Gbps	-	-	Low flexibility, complex receiver, costly
Hybrid FSO/RF system [14]	Monte Carlo simulations	Not used	3000 m	-	-	Clear air, haze, heavy rain	Limited distance
Dense WDM [32]	OptiSim Simulator	30 m	Not used	8 × 40 Gbps	-	-	Limited transmission range
WDM-PON using fiber-FSO [15]	Experimental	25 km (SMF)	2 m	28 Gbps	-	-	Limited wireless range, limited capacity
WDM fiber-FSO [16]	TracePro Simulator	51 km (SMF)	940 m	40 Gbps	-	-	Limited system capacity, low data rate
Ring architecture FSO-fiber [33]	OptiSystem Simulator	20 km (SMF)	700 m	40 Gbps	-	Clear, Light haze, Light rain, heavy rain, Medium rain	Limited capacity, costly
OFDM WDM PON-FSO [1]	OptiSystem Simulator	20 km (SMF)	3000 m	10 Gbps	-	Haze, heavy rain, weak, moderate and strong turbulence	High complexity, low data rate, low capacity
This work	OptiSystem Simulator	3000 m (MMF)	100 m	16 × 10 Gbps	LP_{01}, LP_{22}, LP_{03}, LP_{13}	Clear air, haze, heavy rain, wet snow, weak turbulence	Limited distance

Table 5 depicts the comparative analysis of the obtained results in terms of the insertion loss, gain, received power, output noise, noise figure and beam divergence for different works and the proposed work. Empty spaces indicate that no results were obtained for a particular parameter. As seen, the proposed work offers the highest received power of −12.32 dBm, as compared to other works. A higher received power indicates a stronger signal. The proposed design can sustain a maximum insertion loss of 7.5 dB at BER of 10^{-9}, which is higher than Refs. [8,15,33,34]. However, Ref. [16] offers an acceptable BER performance of 10×10^{-3} with a higher 24.8 dB insertion loss than the proposed work, on account of a lower received power and without a beam divergence effect, compared to the latter. Further, low noise is desirable for optical networks. As compared to Refs. [14,32], the proposed system indicates an acceptable noise of 10 dB, by considering the beam divergence and geometric loss in the FSO link. The proposed system also offers a high gain of −10 dB with a low output noise of −62.66 dBm, neither of which is measured in previous works.

Table 5. Comparison analysis based on obtained results.

Design	Maximum Insertion Loss (dB)	Link Loss (dB)	Received Power (dBm)	Output Noise (dBm)	Spectral Efficiency	Complexity	Noise (dB)	Beam Divergence (mrad)	BER
GPON-MDM [8]	2.5	-	−26	-	Low	Low	-	-	10^{-3}
WDM using fiber–FSO link [34]	7	-	−32.8	-	High	High	-	-	10^{-9}
Hybrid FSO/RF system [14]	-	-	-	-	Low	High	5	-	10^{-3}
DWDM [32]	-	-	-	-	High	Low	4.3	-	10^{-9}
WDM-PON using fiber–FSO [15]	3	-	−35.5	-	Moderate	High	-	-	10^{-3}
PON [13]	3	-	−14	-	High	High	-	-	10^{-3}
WDM fiber–FSO [16]	24.8	-	−32.5	-	Low	High	-	-	10^{-3}
Ring architecture FSO–fiber [33]	6	-	−23.65	-	High	High	-	-	10^{-9}
This work	7.5	−10	−12.32	−62.66	High	Low	10	2	10^{-9}

4. Discussion

In summary, it is observed that using an integrated MMF-FSO link for transmitting different LP modes shows that LP modes can be effectively transmitted up to 3000 m with an MMF link with 100 m FSO at a high spectral efficiency of 16 × 10 Gbps. The proposed system offers better performance compared to the previous works [1,8,9,11,13–16,32,33], considering fiber impairments, free-space loss (clear air, haze, heavy rain, wet snow, weak turbulence), divergence loss, and photodiode losses. It offers reliable high-speed communication with high received power and low noise. However, certain issues have also been identified, such as that the system performance deteriorates under moderate-to-strong turbulence conditions, and the transmission range is limited owing to atmospheric attenuation, different weather conditions, and modal crosstalk. In addition, increasing the number of LP modes may introduce higher system complexity as well as alignment sensitivity.

5. Conclusions

In this work, the ability of an enhanced capacity MDM system over a fiber–FSO integrated link with sixteen transmitted spatial modes, each carrying LP mode, is presented. By employing switch selection at both the transmitter and receiver, the BER of the system goes down to a 10^{-9} threshold at a 160 Gbps aggregate data rate. The system undergoes acceptable BER performance with a maximum insertion loss of 6.4–7.5 dB at LP_{01}, 3.8–5 dB at LP_{22}, 1.5–2.7 dB at LP_{03} and approximately 1–1.5 dB at LP_{13} modes under the impact of clear air, moderate haze, heavy rain and wet snow climates over 100 m FSO and a 100 m PIMMF range. Moreover, the fiber length can be extended up to 2100–3000 m at all operating modes for 1550–1552.4 nm wavelengths. However, the optimum performance can be measured at the LP_{01} mode, which offers a maximum link loss of −10 to −14.70 dB, a high output signal of −7.62 to −12.32 dBm, and low noise of 10 to 14.7 dB. In comparison to existing systems, the proposed architecture offers higher capacity and a higher transmission rate over an integrated fiber–FSO range without using an amplifier under various fiber–FSO link impairments. Moreover, the maximum received power, lower noise level, and an acceptable noise with moderate link loss is obtained, compared to earlier works. It is also analysed that the proposed system offers an acceptable insertion loss level along with FSO link misalignments as compared to the existing works and can be utilized for various fiber fault detection and high capacity 5G and beyond 5G networks.

Again, this work can be extended to moderate-to-strong turbulence conditions by incorporating a larger number of modes. It is realized that FSO link utilization at the front-end network of the proposed MDM-based system increases the system's reliability significantly compared to existing fiber–wireless systems. This system can be employed for large geographical areas providing cost-effectiveness, high-speed, high spectral efficient and high-capacity services.

Author Contributions: M.K., J.M. and S.K.M. discussed the plan and agreed on it. M.K. and J.M. drafted designs for the manuscript. The original manuscript was written by M.K. The manuscript was edited by S.K.M. All authors reviewed and commented on the original draft of the manuscript. All authors have read and agreed to the published version of the manuscript.

Funding: S.K.M wants to thank CTTC for providing the resources to conduct this research. This research is part of SOFIA PID2023-147305OB-C32, funded by MICIU/AEI/10.13039/501100011033 and FEDER/UE.

Institutional Review Board Statement: Not applicable.

Informed Consent Statement: Not applicable.

Data Availability Statement: Data are contained within the article.

Conflicts of Interest: The authors declare no conflicts of interest.

References

1. Ullah, R.; Ullah, S.; Imtiaz, W.A.; Khan, J.; Shah, P.M.A.; Kamran, M.; Ren, J.; Chen, S. High-Capacity Free Space Optics-Based Passive Optical Network for 5G Front-Haul Deployment. *Photonics* **2023**, *10*, 1073. [CrossRef]
2. Li, Y.; Chen, Z.; Hu, Z.; Benton, D.M.; Ali, A.A.I.; Patel, M.; Lavery, M.P.J.; Ellis, A.D. Enhanced Atmospheric Turbulence Resiliency With Successive Interference Cancellation DSP in Mode Division Multiplexing Free-Space Optical Links. *J. Light. Technol.* **2022**, *40*, 7769–7778. [CrossRef]
3. Ci, Y.; Ren, F.; Lei, X.; Li, Y.; Zhou, D.; Wang, J. A Weakly-Coupled Double Bow-Tie Multi-Ring Elliptical Core Multi-Mode Fiber for Mode Division Multiplexing across C+L+U Band. *Appl. Sci.* **2023**, *13*, 5855. [CrossRef]
4. Bremer, K.; Alwis, L.S.M.; Zheng, Y.; Roth, B.W. Towards Mode-Multiplexed Fiber Sensors: An Investigation on the Spectral Response of Etched Graded Index OM4 Multi-Mode Fiber with Bragg Grating for Refractive Index and Temperature Measurement. *Appl. Sci.* **2020**, *10*, 337. [CrossRef]
5. Amirabadi, M.A.; Nezamalhosseini, S.A.; Kahaei, M.H.; Chen, L.R. Improving MDM–WDM Optical Network Performance via Optimized Power Allocation Using Gaussian Noise Model. *Opt. Fiber Technol.* **2023**, *75*, 103187. [CrossRef]
6. Zhang, R.; Tang, X.; Hsu, C.W.; Chen, Y.W.; Chang, G.K. Semi-Supervised and Supervised Nonlinear Equalizers in Fiber-FSO Converged System. *J. Light. Technol.* **2021**, *39*, 6175–6181. [CrossRef]
7. Singh, P.; Bohara, V.A.; Srivastava, A. Reliable and Cost Effective All-Optical Wireless Architecture for a Broadband Access Network. *J. Opt. Commun. Netw.* **2023**, *15*, 98–110. [CrossRef]
8. Hu, T.; Li, J.; Zhang, Y.; Li, Z.; He, Y.; Chen, Z. Wavelength-Insensitive Weakly Coupled FMFs and Components for the MDM-GPON. *IEEE Photonics Technol. Lett.* **2018**, *30*, 1277–1280. [CrossRef]
9. Chen, Y.; Li, J.; Zhou, P.; Zhu, P.; Tian, Y.; Wu, Z.; Zhu, J.; Liu, K.; Ge, D.; Chen, J.; et al. MDM-TDM PON Utilizing Self-Coherent Detection-Based OLT and RSOA-Based ONU for High Power Budget. *IEEE Photonics J.* **2016**, *8*, 7904207. [CrossRef]
10. Ren, F.; Li, J.; Hu, T.; Tang, R.; Yu, J.; Mo, Q.; He, Y.; Chen, Z.; Li, Z. Cascaded Mode-Division-Multiplexing and Time-Division-Multiplexing Passive Optical Network Based on Low Mode-Crosstalk FMF and Mode MUX/DEMUX. *IEEE Photonics J.* **2015**, *7*, 7903509. [CrossRef]
11. Minoofar, A.; Su, X.; Zhou, H.; Zhang, R.; Alishahi, F.; Zou, K.; Song, H.; Pang, K.; Zach, S.; Tur, M.; et al. Experimental Demonstration of Sub-THz Wireless Communications Using Multiplexing of Laguerre-Gaussian Beams When Varying Two Different Modal Indices. *J. Light. Technol.* **2022**, *40*, 3285–3292. [CrossRef]
12. Sinha, S.; Kumar, C. Evaluation of a High-Speed Hybrid OAM-OFDM-MDM Multiplexed Coherent FSO System under Desert Conditions. *Opt. Appl.* **2023**, *LIII*, 431–445. [CrossRef]
13. Yeh, C.; Chow, C.; Yang, M.; Hsu, D. A Flexible and Reliable 40-Gb/s OFDM Downstream TWDM-PON Architecture. *IEEE Photonics J.* **2015**, *7*, 7905709. [CrossRef]
14. Sharma, S.; Madhukumar, A.S.; Swaminathan, R. Switching-Based Cooperative Decode-and-Forward Relaying for Hybrid FSO/RF Networks. *J. Opt. Commun. Netw.* **2019**, *11*, 267–281. [CrossRef]

15. Yeh, C.H.; Wang, B.Y.; Hsu, W.H.; Liu, L.H.; Ko, H.S. A Simple WDM-PON Architecture Together with Private Interconnected ONUs. *IEEE Access* **2021**, *9*, 126319–126323. [CrossRef]
16. Yeh, C.H.; Chen, J.R.; You, W.Y.; Chow, C.W. Hybrid WDM FSO Fiber Access Network with Rayleigh Backscattering Noise Mitigation. *IEEE Access* **2020**, *8*, 96449–96454. [CrossRef]
17. Wu, Z.; Li, J.; Tian, Y.; Ge, D.; Zhu, J.; Ren, F.; Mo, Q.; Yu, J.; Li, Z.; Chen, Z.; et al. Fundamental-Mode MMF Transmission Enabled by Mode Conversion. *Opt. Commun.* **2018**, *410*, 112–116. [CrossRef]
18. Fazea, Y.; Mezhuyev, V. Selective Mode Excitation Techniques for Mode-Division Multiplexing: A Critical Review. *Opt. Fiber Technol.* **2018**, *45*, 280–288. [CrossRef]
19. Li, J.; Ren, F.; Hu, T.; Li, Z.; He, Y.; Chen, Z.; Mo, Q.; Li, G. Recent Progress in Mode-Division Multiplexed Passive Optical Networks with Low Modal Crosstalk. *Opt. Fiber Technol.* **2017**, *35*, 28–36. [CrossRef]
20. Muciaccia, T.; Gargano, F.; Passaro, V. Passive Optical Access Networks: State of the Art and Future Evolution. *Photonics* **2014**, *1*, 323–346. [CrossRef]
21. Agrawal, G.P. *Applications of Nonlinear Fiber Optics*; Academic Press: Cambridge, MA, USA, 2010.
22. Yu, S.; Ding, J.; Fu, Y.; Ma, J.; Tan, L.; Wang, L. Novel Approximate and Asymptotic Expressions of the Outage Probability and BER in Gamma–Gamma Fading FSO Links with Generalized Pointing Errors. *Opt. Commun.* **2019**, *435*, 289–296. [CrossRef]
23. Ahmad Anas, S.B.; Hamat, F.H.; Hitam, S.; Sahbudin, R.K.Z. Hybrid Fiber-to-the-x and Free Space Optics for High Bandwidth Access Networks. *Photonic Netw. Commun.* **2012**, *23*, 33–39. [CrossRef]
24. Mohsan, S.A.H.; Khan, M.A.; Amjad, H. Hybrid FSO/RF Networks: A Review of Practical Constraints, Applications and Challenges. *Opt. Switch. Netw.* **2023**, *47*, 100697. [CrossRef]
25. Niaz, A.; Qamar, F.; Ali, M.; Farhan, R.; Islam, M.K. Performance Analysis of Chaotic FSO Communication System under Different Weather Conditions. *Trans. Emerg. Telecommun. Technol.* **2019**, *30*, e3486. [CrossRef]
26. Al-Gailani, S.A.; Mohd Salleh, M.F.; Salem, A.A.; Shaddad, R.Q.; Sheikh, U.U.; Algeelani, N.A.; Almohamad, T.A. A Survey of Free Space Optics (FSO) Communication Systems, Links, and Networks. *IEEE Access* **2021**, *9*, 7353–7373. [CrossRef]
27. Kassim, A.Y.; Oduol, V.K.; Usman, A.D. Design and Performance Evaluation of a 350 m Free Space Optical Communications Link for Pico-Macrocell Backhauling. *Int. J. Electr. Comput. Eng.* **2024**, *14*, 2725–2736. [CrossRef]
28. Awan, M.S.; Csurgai-Horváth, L.; Muhammad, S.S.; Leitgeb, E.; Nadeem, F.; Khan, M.S. Characterization of Fog and Snow Attenuations for Free-Space Optical Propagation. *J. Commun.* **2009**, *4*, 533–545. [CrossRef]
29. Kim, I.I. Wireless Optical Transmission of Fast Ethernet, FDDI, ATM, and ESCON Protocol Data Using the TerraLink Laser Communication System. *Opt. Eng.* **1998**, *37*, 3143. [CrossRef]
30. Ghatak, A.K.; Thyagarajan, K. *An Introduction to Fiber Optics*; Cambridge University Press: Cambridge, UK, 1998; pp. 1–565.
31. Brown, G.D. Bandwidth and Rise Time Calculations for Digital Multimode Fiber-Optic Data Links. *J. Light. Technol.* **1992**, *10*, 672–678. [CrossRef]
32. Lavrinovica, I.; Porins, J. Noise Figure Analysis of EDFA with Different Pumping Configurations in 40 Gbit/s 8 Channel DWDM Transmission System. In *2015 Advances in Wireless and Optical Communications, RTUWO 2015*; IEEE: New York, NY, USA, 2015; pp. 34–37.
33. Khare, S.; Kumar Garg, A.; Janyani, V. Ring Based Hybrid FSO- Fiber Optic Architecture Utilizing Same Wavelengths for Downstream and Upstream Transmission with FN/DN Protection Capability. *Opt. Fiber Technol.* **2022**, *73*, 103050. [CrossRef]
34. Garg, A.K.; Janyani, V.; Batagelj, B.; Zainol Abidin, N.H.; Abu Bakar, M.H. Hybrid FSO/Fiber Optic Link Based Reliable & Energy Efficient WDM Optical Network Architecture. *Opt. Fiber Technol.* **2021**, *61*, 102422. [CrossRef]

Disclaimer/Publisher's Note: The statements, opinions and data contained in all publications are solely those of the individual author(s) and contributor(s) and not of MDPI and/or the editor(s). MDPI and/or the editor(s) disclaim responsibility for any injury to people or property resulting from any ideas, methods, instructions or products referred to in the content.